TRANSPLANTATION

Discordance in lymphoid tissue recovery following stem cell transplantation in rhesus macaques: an in vivo imaging study

Robert E. Donahue,[1] Sharat Srinivasula,[2] Naoya Uchida,[3] Insook Kim,[4] Alexis St. Claire,[5] Gorka Duralde,[5] Paula DeGrange,[6] Marisa St. Claire,[6] Richard C. Reba,[7] Aylin C. Bonifacino,[1] Allen E. Krouse,[1] Mark E. Metzger,[1] Chang H. Paik,[8] H. Clifford Lane,[9] John F. Tisdale,[3] and Michele Di Mascio[5]

[1]Hematology Branch, National Heart, Lung, and Blood Institute (NHLBI), National Institutes of Health (NIH), Bethesda, MD; [2]Biostatistics Research Branch, Leidos Biomedical Research, Inc, Frederick National Laboratory for Cancer Research (FNLCR), Frederick, MD; [3]Molecular and Clinical Hematology Branch, NHLBI, NIH, Bethesda, MD; [4]Applied/Developmental Research Directorate, Leidos Biomedical Research, Inc, FNLCR, Frederick, MD; [5]Division of Clinical Research, National Institute of Allergy and Infectious Diseases (NIAID), NIH, Bethesda, MD; [6]Integrated Research Facility, NIAID, NIH, Frederick, MD; and [7]Center for Infectious Disease Imaging, Radiology and Imaging Sciences, Clinical Center, [8]Radiopharmaceutical Laboratory, Nuclear Medicine, Radiology and Imaging Sciences, Clinical Center, and [9]Laboratory of Immunoregulation, NIAID, NIH, Bethesda, MD

Key Points

- Single-photon emission computed tomography imaging can be used to image immune recovery in lymphoid tissues following transplant.
- There is discordance between lymphoid tissues and the peripheral blood in numbers of $CD4^+$ cells following various doses of irradiation.

Ionizing irradiation is used routinely to induce myeloablation and immunosuppression. However, it has not been possible to evaluate the extent of ablation without invasive biopsy. For lymphoid recovery, peripheral blood (PB) lymphocytes (PBLs) have been used for analysis, but they represent <2% of cells in lymphoid tissues (LTs). Using a combination of single-photon emission computed tomography imaging and a radiotracer (^{99m}Tc-labeled rhesus immunoglobulin G1 anti-CD4R1 (Fab′)$_2$), we sequentially imaged $CD4^+$ cell recovery in rhesus macaques following total body irradiation (TBI) and reinfusion of vector-transduced, autologous $CD34^+$ cells. Our results present for the first time a sequential, real-time, noninvasive method to evaluate $CD4^+$ cell recovery. Importantly, despite myeloablation of circulating leukocytes following TBI, total depletion of $CD4^+$ lymphocytes in LTs such as the spleen is not achieved. The impact of TBI on LTs and PBLs is discordant, in which as few as 32.4% of $CD4^+$ cells were depleted from the spleen. In addition, despite full lymphocyte recovery in the spleen and PB, lymph nodes have suboptimal recovery. This highlights concerns about residual disease, endogenous contributions to recovery, and residual LT damage following ionizing irradiation. Such methodologies also have direct application to immunosuppressive therapy and other immunosuppressive disorders, such as those associated with viral monitoring. (*Blood*. 2015;126(24):2632-2641)

Introduction

The therapeutic use of ionizing irradiation is routine and is associated with myeloablation and immunosuppression. This is particularly true in the setting of hematopoietic stem cell transplantation (HSCT). Depending upon the dose of irradiation, the extent of the depletion can be quite severe with the potential for prolonged recovery periods and other adverse events, such as interstitial pulmonary pneumonitis. Successful immune reconstitution without increasing the risk of graft-versus-host disease is critical to diminishing the risk of posthematopoietic cell transplant infections, cancer relapse, and secondary malignancies. Evaluating immune recovery of lymphoid tissues (LTs) following transplantation, immunosuppressive regimens, or viral infections has proven to be problematic without invasive biopsy. Fewer than 2% of the total numbers of lymphocytes are peripheral blood (PB) lymphocytes (PBLs), the majority reside in LTs.[1] Hence, small changes in the distribution of cells between PB and LT (eg, LT homing) could have profound effects on PBL counts.

We and others have established a large animal model for performing gene transfer and HSCT in rhesus macaques.[2] This model has allowed us to evaluate immune recovery of rhesus macaques transplanted with immunoselected $CD34^+$ cells transduced with retroviral vectors. Most recently, we developed a chimeric lentiviral vector containing portions of the HIV and the simian immunodeficiency virus (SIV) which efficiently transduces rhesus $CD34^+$ cells and expresses enhanced green fluorescent protein (EGFP) as a marker to determine the contributions of the transduced $CD34^+$ cells to various elements of the hematopoietic lineage posttransplant.[3] In addition, we have developed a strategy to evaluate noninvasively and in real time the contribution of the $CD4^+$ cell population to LTs using single-photon emission computed tomography (SPECT) imaging.[4] This technique has been used to study the relationships between the PB and LT pool of $CD4^+$ T cells in healthy and SIV- or simian/human immunodeficiency virus (SHIV)-infected animals. In the present study, we have used a combination of SPECT imaging and a radiotracer, ^{99m}Tc-labeled rhesus immunoglobulin G1 (rhIgG1) anti-CD4R1 (Fab′)$_2$, to longitudinally image $CD4^+$ cell recovery in rhesus macaques following varying doses of total body irradiation (TBI) and reinfusion of vector-transduced,

Submitted July 23, 2015; accepted October 14, 2015. Prepublished online as *Blood* First Edition paper, October 22, 2015; DOI 10.1182/blood-2015-07-657346.

The online version of this article contains a data supplement.

The publication costs of this article were defrayed in part by page charge payment. Therefore, and solely to indicate this fact, this article is hereby marked "advertisement" in accordance with 18 USC section 1734.

autologous $CD34^+$ cells to determine the impact of these modalities on $CD4^+$ T-cell depletion and recovery. This is especially important in graft rejection, as it has been previously shown that clonable, alloreactive host T cells can be recovered from the spleen of rhesus macaques following hyperfractionated TBI and chemotherapy.[5]

Methods

Animals

Eleven rhesus macaques (*Macaca mulatta*) were used following National Heart, Lung, and Blood Institute (NHLBI) and National Institute of Allergy and Infectious Diseases (NIAID) Animal Care and Use Committee approved protocols. Eight rhesus macaques (supplemental Table 1, see supplemental Data available on the *Blood* Web site) were irradiated and transplanted; 7 were imaged pre- and posttransplant, and 6 underwent longitudinal imaging (supplemental Figure 2). Two (ZI10 and ZI12) received a dose of 3 Gy on 2 sequential days (3Gyx2) of TBI (6 Gy total), 3 (ZG21, ZH32, and ZG41) received a dose of 4 Gy on 2 sequential days (4Gyx2) of TBI, and 3 (ZG70, ZI64, and ZJ37) received a dose of 5 Gy on 2 sequential days (5Gyx2) of TBI. ZI10 developed an antibody response to the radiotracer and could not be reimaged posttransplant. ZI64 was euthanized on day 6 posttransplant following SPECT imaging and LTs were collected for evaluation. One rhesus macaque (G43) in chronic stage, coinfected with SIV/SHIV lentivirus, with very low PB $CD4^+$ T-cell counts was imaged to serve as a positive control. In addition, 2 long-term transplanted animals (RQ7280 and RQ7387) having received 5Gyx2 TBI were imaged. The 4Gyx2 TBI animals were also imaged during mobilization with AMD3100 (Sigma-Aldrich), administered at 1 mg/kg subcutaneously (SQ).

Transplant

$CD34^+$ cells were immunoselected from a leukapheresis product following granulocyte colony-stimulating factor (G-CSF) and stem cell factor (SCF) mobilization over 5 days as previously described.[2] On the last day of irradiation autologous $CD34^+$ cells were reinfused after being transduced once (multiplicity of infection [MOI] = 50) with a SIV/HIV chimeric lentiviral vector expressing EGFP.[3]

Preparation of $F(ab')_2$ anti-CD4 antibodies

To produce rhesus recombinant antibody, CD4R1-OKT4A/rhIgG1, complementarity determining regions (CDRs) representing the anti-CD4 antibody OKT4A[6] were grafted onto a rhesus scaffold using the rhesus germline variable region as templates. Key positions potentially contributing to antigen binding, CDR conformation, and heavy-light chain interactions were retained as the mouse residue.[7] DNA representing recombinant variable heavy and variable light chains were synthesized, amplified by polymerase chain reaction, and purified from agarose gel with the QIAquick Gel Extraction kit (Qiagen). For large-scale production of rhesus recombinant antibodies, recombinant heavy- and light-chain vectors were packaged in retroviral vectors and used to infect CHO cells using the GPEx expression platform (Catalent Pharma Solutions). Antibody was produced from a high-expressing transduced subclone, grown in serum-free medium. After clarification, recombinant antibody was purified from supernatant by protein A affinity chromatography. The purified antibodies were placed in phosphate buffer, pH 6.5. Endotoxin levels were <1 endotoxin unit (EU)/mg of antibody.

$F(ab')_2$ fragments of CD4R1-OKT4A/rhIgG1 monoclonal antibodies (mAbs) ($F(ab')_2$-CD4R1) were prepared by pepsin digestion according to the manufacturer's instructions (Thermo Scientific). After digestion, the reaction mixture was purified using protein A-Sepharose affinity chromatography (Thermo Scientific), followed by dialysis in phosphate-buffered saline (PBS) using a dialysis membrane cassette with 20-kDa molecular weight cutoff at 4°C for 22 hours, and concentrated using a Centriprep YM-50 membrane (Amicon) to a concentration of 5.2 mg/mL. Protein purity was assessed by sodium dodecyl sulfate–polyacrylamide gel electrophoresis (Invitrogen) and size-exclusion high-performance liquid chromatography (HPLC; Gilson) equipped with a size-exclusion TSK gel G3000SWXL column (7.8 × 300 mm, 5 μm [TOSOH Bioscience]; 0.067 M sodium phosphate/0.15 M sodium chloride, pH 6.8; 1.0 mL per minute) and an ultraviolet monitor.

Conjugation of HYNIC to $F(ab')_2$-CD4R1

Succinimidyl 6-hydraziniumnicotinate hydrochloride (HYNIC-NHS; Solulink) was freshly dissolved in dimethylformamide (5.2 mM). Ten times molar excess (200 μmol) of HYNIC-NHS was added to 2 mg (20 μmol) of $F(ab')_2$ fragments in 0.4 mL of 0.0067 M PBS buffer (PBS 1×), pH 7.2. The solution was stirred gently and incubated in a refrigerator at 4°C for 65 hours. The level of HYNIC conjugation was estimated to be 3 HYNIC molecules per $F(ab')_2$ by the percentage of distribution of ^{99m}Tc between HYNIC-$F(ab')_2$ and free HYNIC when analyzed by size-exclusion HPLC. The reaction mixture was diluted 10 times with the same PBS and concentrated by Amicon 50K. The conjugated product was stored in a freezer at −80°C until radiolabeling with ^{99m}Tc for imaging studies.

^{99m}Tc labeling

In a rubber-sealed vial, HYNIC-$F(ab')_2$ -CD4R1 (360 μg in PBS 1×) was incubated with $^{99m}TcO_4^{-1}$ (40 mCi; 1480 MBq) in 0.2 mL of aqueous medium at pH 6 containing tricine (112 mM, 20 mg/mL), sodium succinate (25 mM), and stannous chloride (82 μg/mL) at room temperature for 30 minutes. All reagents were freshly made in deionized water which was deoxygenized by bubbling with N_2 stream for 1 hour. ^{99m}Tc-labeled $F(ab')_2$ proteins were purified on PD-10 size-exclusion column (GE Healthcare) eluted with PBS, pH 7.2. The radiochemical purity of the ^{99m}Tc-labeled $F(ab')_2$ was determined by size-exclusion HPLC equipped with an online flow radioactivity detector (BioScan). The specific activity of the labeled fragments at the time of injection was >41 mCi/mg. Radiochemical purity >90% was used for both in vitro and in vivo imaging studies.

CD4 cell-binding assays

The immunoreactivity of the radiolabeled products was tested using a modification of a cell-binding assay described by Lindmo and Bunn,[8] as previously described.[4]

Imaging and biodistribution studies

SPECT/computed tomography (CT) images were taken prior to transplant and at ~6, 30, 90, 150, 260, and 380 days post-TBI. Animals were anesthetized with ketamine (10 mg/kg), and maintained on propofol (Diprivan 10 mg/mL; initial 2.5-5 mg/kg dose given as a bolus, then 0.3-0.4 mg/kg per minute of constant IV infusion). Injected doses of ^{99m}Tc -$F(ab')_2$-CD4R1 are reported in supplemental Table 2. Serial scintillation camera images were acquired with the dual-headed SPECT-CT camera (Symbia T2; SPECT/CT Siemens) at 4 hours postradiotracer injection. The images were obtained with a low-energy high-resolution collimator. SPECT images were analyzed from 2 independent operators by manually drawing consecutive regions of interest (ROIs) over the transversal sections of the heart, liver, kidney, bone marrow (a first ROI was positioned over the proximal segment of the humerus [proximal humerus] and a second ROI was positioned in the center of the humerus [central humerus]), thymus, submandibular, axillary and inguinal lymph nodes (LNs), and spleen to cover the entire volume of the organs (volume of interest [VOI]). The VOI for the submandibular LNs may also include salivary glands. The coregistration of CT and SPECT images was used to confirm the VOI of the above organs. To estimate the relative retention of radiotracers in different organs, semiquantitative analysis of SPECT images was performed on 3-dimensional-reconstructed and whole-body images obtained at 4 hours postradiotracer injection. Images were not corrected for partial volume effect. The retention of radiotracer for each VOI was obtained from the maximum activity in the VOI minus the background activity in a VOI placed close to the organ, and normalized on the maximum activity in the liver. In addition, hepatic and other tissue radiotracer uptakes were measured as maximum standardized uptake value (SUVmax) from the SPECT images. At the end of each imaging study, 500 μL of blood was withdrawn for whole blood and plasma radioactivity counting in the γ counter. No association was found between liver uptake (SUVmax), whole blood, or plasma SUV and number of $CD4^+$ cells per μL ($P > .05$) in the entire group of 11 animals imaged (baseline

CD4 count range, 7-1784). This lack of association was confirmed in a larger group of 31 healthy and SIV/SHIV-infected animals (baseline CD4 count, 7-2335/μL) (S.S. and M.D.M., unpublished data). The association between radiotracer uptake in kidney, heart, thymus, and bone marrow (proximal and central humerus) and PB CD4 count (using both retention and SUV as mathematical operators) was not statistically significant. This suggests that the majority of the radiotracer uptake in these organs was the result of nonspecific uptake. In contrast, highly statistically significant associations were observed between radiotracer uptake in LTs (spleen and clusters of LNs) and the PB CD4 count ($P < .01$, n = 31), suggesting that the majority of the radiotracer uptake in these organs is the result of specific uptake.[9] Development of immunogenicity to the radiotracer was monitored using size-exclusion HPLC and an in vitro cell-binding assay. Baseline and postmobilization (with 1 mg/kg AMD3100 SQ) SPECT/CT images were taken at least 2 months prior to transplantation for the 4Gyx2 TBI monkeys.

Immunogenicity assays

Plasmas at each imaging time point were screened for antibodies to the probe and data were excluded from the analyses if animals developed an anti-anti-CD4 immune response. Two independent assays were performed to assess immunogenicity: radio-HPLC analysis and MT4 cell-binding assay with plasma preincubated with the radiotracer. Aliquots of ^{99m}Tc -F(ab′)$_2$-CD4R1 were incubated in monkey plasma to reach similar activity concentration to in vivo plasma concentration at 4 hours postradiotracer injection (~0.1 ng/μL), for 30 minutes at 37°C in a humidified 5% CO_2 incubator. The aliquot of samples were analyzed by size-exclusion HPLC equipped with an online flow radioactivity detector using a TSK gel G3000SWXL column (7.8 × 300 mm, 5 μm; TOSOH Bioscience) with mobile-phase 0.067 M sodium phosphate/0.15 M sodium chloride (pH 6.8; 1.0 mL per minute). Another 20 μL of the radiotracer-plasma incubation mixtures under the above conditions were also dispensed in 2 million MT4 cells and incubated for 90 minutes at 4°C for the plasma cell-binding assay. After incubation, the wells were washed, and the percentage of total activity bound to cells was determined in a γ counter (Wizard).

Flow cytometry

Transduced rhesus CD34$^+$ cells were cultured for an additional 3 to 4 days in vitro and EGFP expression was evaluated by FACSCalibur (BD Biosciences). After transplantation, EGFP and cell surface marker expression of rhesus PB cells were analyzed using CD4-conjugated allophycocyanin (APC) (clone L200), CD8-phycoerythrin (PE), or PE-Cy^7 (clone RPA-T8), and CD20-APC or PE (clone 2H7; all BD Pharmingen). CD34$^+$ cells were assessed for purity using a mouse anti-human CD34-PE (clone 563; BD Pharmingen). Stained cells were analyzed by a Cytomics FC500 (Beckman Coulter). Absolute numbers were calculated by white blood cell count multiplied by the percentages of CD4, CD8, or CD20 within the lymphocyte gate.

Ex vivo analyses

For ZI64, the spleen, and axillary, inguinal, and submandibular LNs were removed at 6 hours following ^{99m}Tc-F(ab′)$_2$-CD4R1 injection. LNs and spleen aliquots were mechanically disrupted by pressing through a 70-μm pore-size cell strainer (Fisher Scientific). Erythrocytes were lysed with ACK lysing buffer (BioWhittaker), and cells washed with RPMI 1640 (Lonza). Isolated cells were resuspended in 1 mL of PBS and radioactivity counted in the γ counter.

Immunohistochemistry

Fixed embedded tissues sections from LNs and spleen of ZI64 at day 6 post-TBI, LNs from ZG21, ZH32, and ZG41 at year 1 post-TBI, and LNs and spleen from healthy controls were stained with rabbit polyclonal anti-human CD3 antibody (DakoCytomation). Sections were deparaffinized and rehydrated with 4 changes of xylene and 1 change of graded ethanol for 5 minutes each followed by pretreatment for 20 minutes at 85°C. The samples were sequentially treated with PBS, aqueous hydrogen peroxide, serum block (bovine serum albumin), the primary anti-CD3 antibody (1/100 dilution), and the secondary antibody biotin-conjugated goat anti-rabbit antibody (DakoCytomation). The reaction was visualized by using the AES substrate kit (Vector Laboratories). Samples were then rinsed in distilled water and counterstained with hematoxylin. Bright-field images of stained tissue sections were acquired using a Leica Epi microscope (Leica).

Statistical methods

The significance of paired differences (within each group) was determined by *t* test. All *P* values are 2-sided. The correlation between radiotracer uptake and CD4$^+$ cell count in the PB was tested with the Spearman rank correlation test.

Results

In vitro binding and ex vivo studies

Binding inhibition with excess amounts of the cold mAbs was ~99% of the total incubated radioactivity and was independent of the concentration of radiotracer, suggesting that the radioactivity trapped in the cell pellet of MT4 cells was the result of specific binding of the radiotracer (supplemental Figure 1). The percentage of the labeled fragment bound to cells was >60% at 4 × 10^6 MT4 cells, and its immunoreactivity was estimated to be ~100% extrapolated under condition of excess receptor concentration based on the Lindmo method,[8] similar to the intact anti-CD4 mAbs previously described.[4] In order to demonstrate the specificity of radiotracer binding to CD4$^+$ cells in vivo, CD4$^+$ cells were isolated from the LNs of 2 monkeys 4 hours after the administration of radiotracer (^{99m}Tc -F(ab′)$_2$-CD4R1) and the total radioactivity associated with the CD4$^+$ and CD4$^-$ cells determined. The levels of the radiotracer associated with the CD4$^+$ cells were consistently higher than the levels of the radiotracer in the CD4$^-$ cells (mean ratio, ~10) thus showing specificity of binding to CD4$^+$ cells, consistent with our previous observations using the parent radiotracer ^{111}In-DTPA-CDR-OKT4A/huIgG4.[4,9] The size-exclusion HPLC analysis of the plasma at baseline imaging showed that ~90% of the injected ^{99m}Tc -F(ab′)2-CD4R1 remained at ~4 hours postinjection in vivo, and no evidence of formation of metabolites or catabolites, thus confirming the stability of the radiotracer in vivo (data not shown).

AMD3100 mobilization

To determine the impact of PBL mobilization on imaging, 3 monkeys (ZG21, ZH32, and ZG41) were imaged during mobilization with AMD3100. Previously, we have shown that AMD3100 effectively mobilizes a wide variety of lymphocyte subsets into the PB.[10] Baseline SPECT images were taken prior to mobilization and then dynamic planar acquisitions were acquired for 2 hours postmobilization with 1 mg/kg AMD3100 SQ followed by SPECT images. These images (Figure 1A-B) did not reveal measurable changes in the whole-body CD4 pool, despite an approximately twofold maximum increase in CD4$^+$ PB cell counts (supplemental Figure 3). This observation is consistent with a small percentage of CD4$^+$ cells being released from tissues to PB without significantly affecting lymphocyte pools in the whole body.

In vivo imaging studies

CD34$^+$ cells were immunoselected from a leukapheresis product following 5 days of G-CSF and SCF mobilization. On the last day of TBI, autologous CD34$^+$ cells were reinfused after being transduced once (MOI = 50) with a SIV/HIV chimeric lentiviral vector expressing EGFP.[3] SPECT/CT images were taken prior to transplant and at ~1 week, 1, 3, 5, and 9 months, and 1 year post-TBI (supplemental Figure 2). Development of immunogenicity to the radiotracer was monitored using size-exclusion HPLC and an in vitro cell-binding assay in plasma at each imaging time point (Figure 2). Data were

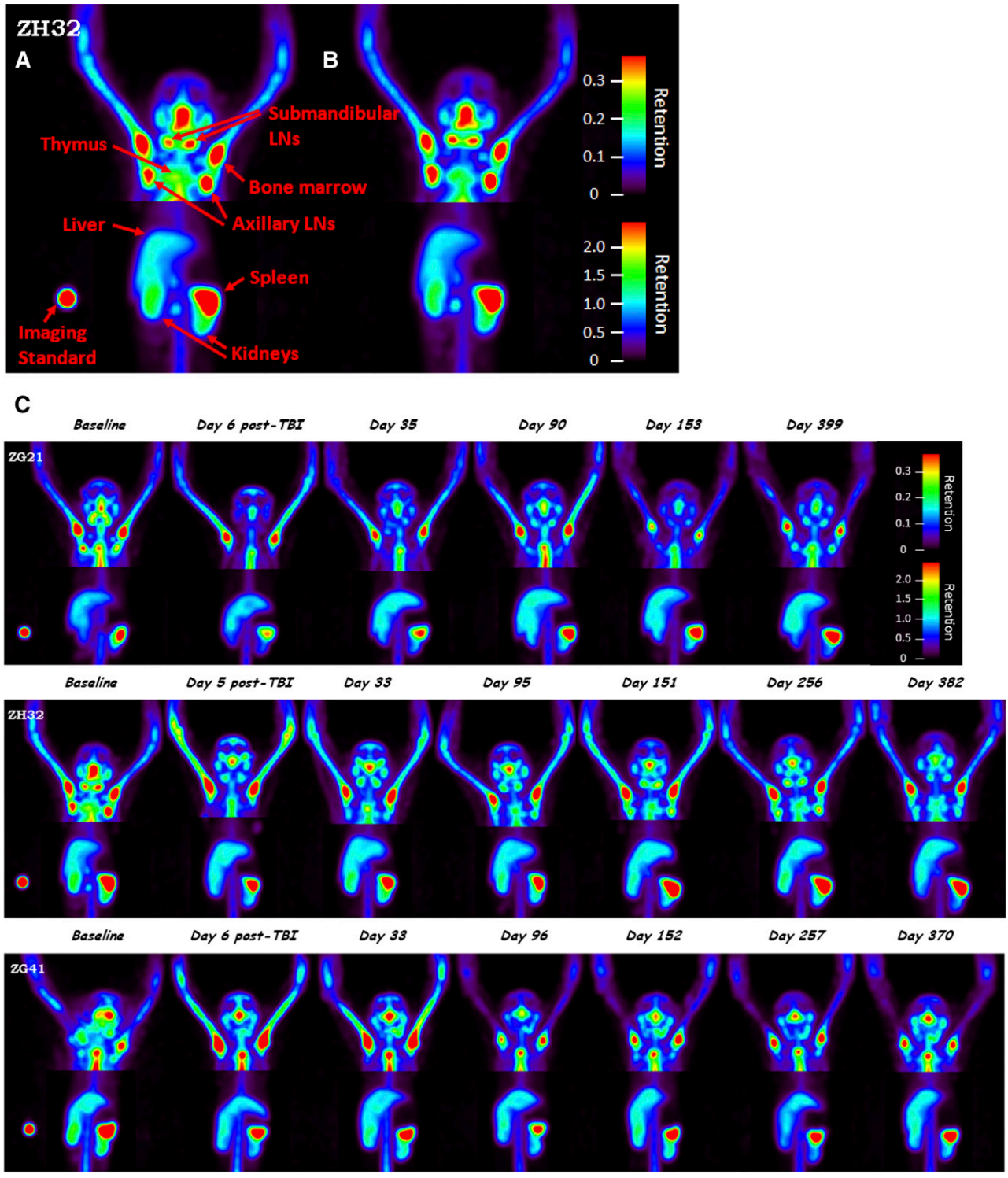

Figure 1. Evaluation of CD4$^+$ cells in tissues for 4Gyx2 TBI-transplanted monkeys. Baseline (A) and 2 hours postmobilization with AMD3100 (B) SPECT maximum intensity projection image of ZH32 with arrows pointing to specific tissues along with imaging standard. Baseline and longitudinal SPECT maximum intensity projection images (C) for up to 1 year following TBI of ZG21, ZH32, and ZG41 rhesus macaques. All images are adjusted within and among monkeys on the maximum liver uptake. Different image contrasts were applied to head and abdominal field of views to highlight clusters of LNs and spleen. Grayscale images were converted to rainbow colors with appropriate retention scales, where red color indicates high retention.

excluded from the analyses if the animals developed an antibody response to the probe.

Following 3Gyx2 TBI, both animals rejected their CD34$^+$ cell graft (supplemental Figure 4) despite achieving a PBL nadir of $<$150 lymphocytes per μL. In both animals, we observed a very high percentage (close to 100%) of EGFP-positive cells predominantly among the granulocyte fraction 1 to 3 months after transplantation (supplemental Figure 4). As we have reported elsewhere, the presence

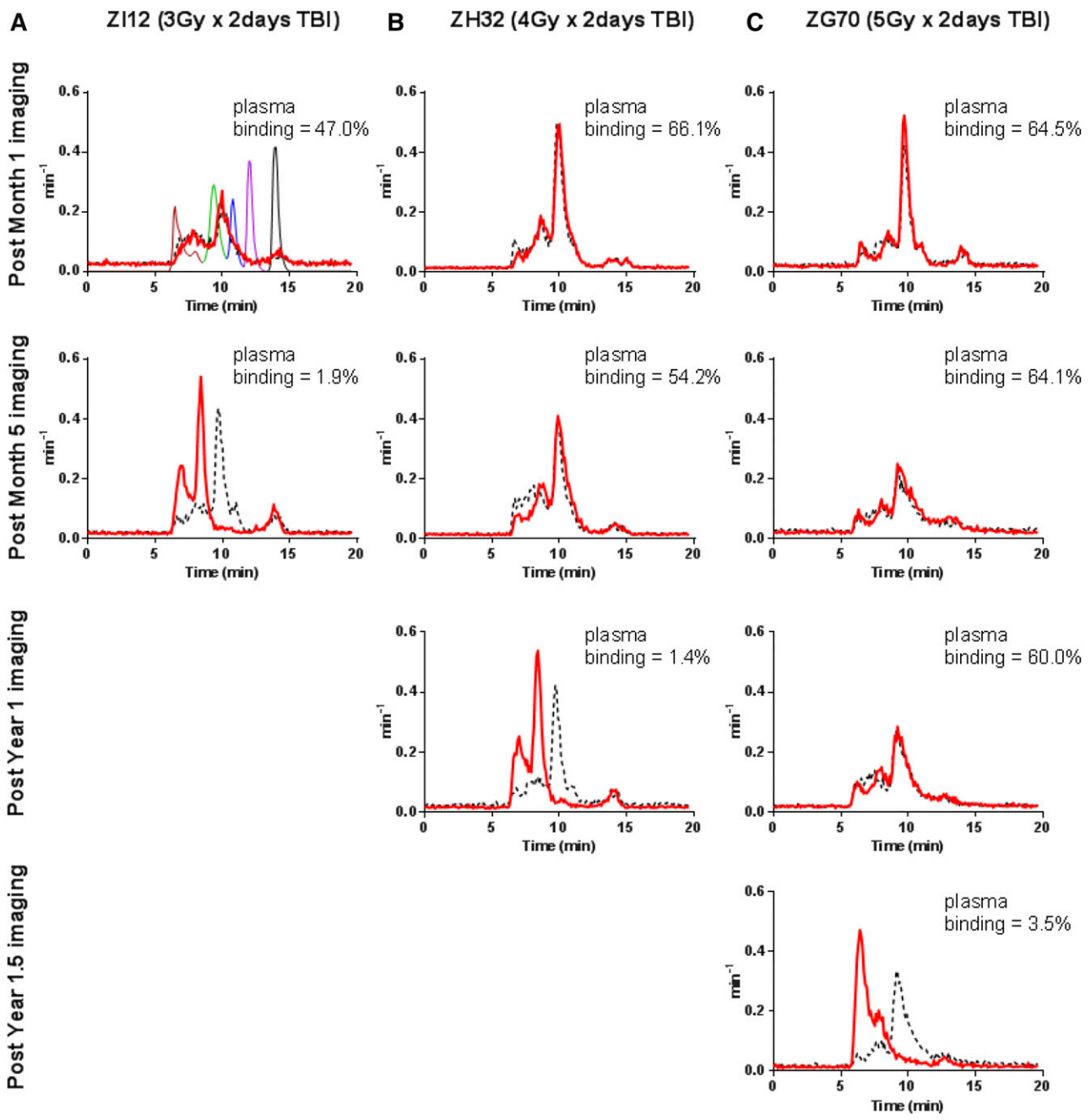

Figure 2. Immune response to the radiotracer. Formation of high-molecular-weight immune complexes in plasma can be detected by HPLC as early as 3 to 4 weeks following incubation with the radiotracer. Radiochromatograms were transformed into probability density curves by normalizing for the area under the curve. Development of the immune response was dependent on TBI dose. (A) For monkeys who received 3Gyx2 TBI it is rapid, within 3 to 4 weeks or 7 months. (B) For 4Gyx2 TBI monkeys, the immune response is delayed, occurring approximately around 1 year post-TBI. (C) For 5Gyx2, an immune response to the radiotracer appears at 1.5 years. HPLC chromatograms are in parallel with the plasma-binding assay results (shown as an inset in each HPLC histogram). As a negative control, plasma from an unexposed monkey (black dash) was run through HPLC on the same day in addition to gel-filtration HPLC standard mixture (as shown in first panel) containing 5 standard components with different molecular weights (MW) (bovine thyroglobulin [MW 670 000 Da; brown], bovine γ-globulin [MW 158 000 Da; green], chicken ovalbumin [MW 44 000 Da; blue], horse myoglobin [MW 17 000 Da; purple], and vitamin B12 [MW 1350 Da; black]).

of high titers of anti-EGFP antibody production in these animals[11] and positive mixed lymphocyte cultures in response to GFP stimulators in others who received 4 Gy TBI,[12] are consistent with rejection based on both cell-mediated and humoral immunity. Both animals also developed an immune response to the radiotracer, one (ZI10) within 4 weeks of the baseline scan and the other (ZI12) within 7 months following TBI. Unlike the 3Gyx2 TBI animals, no immunogenicity to the radiotracer was detected in the 4Gyx2 TBI rhesus monkeys until at least 1 year posttransplant (Figure 2). After the sixth or seventh exposure, all 3 animals developed an immune response to the radiotracer. This suggests immune recovery remained incomplete in the animals receiving a dose of 4Gyx2 TBI for at least 1 year following transplant. Similarly, an immune response to the radiotracer was observed at 1.5 years for ZG70 (Figure 2) using both the plasma MT4-binding assay and by HPLC despite a continued tolerance to EGFP expression.

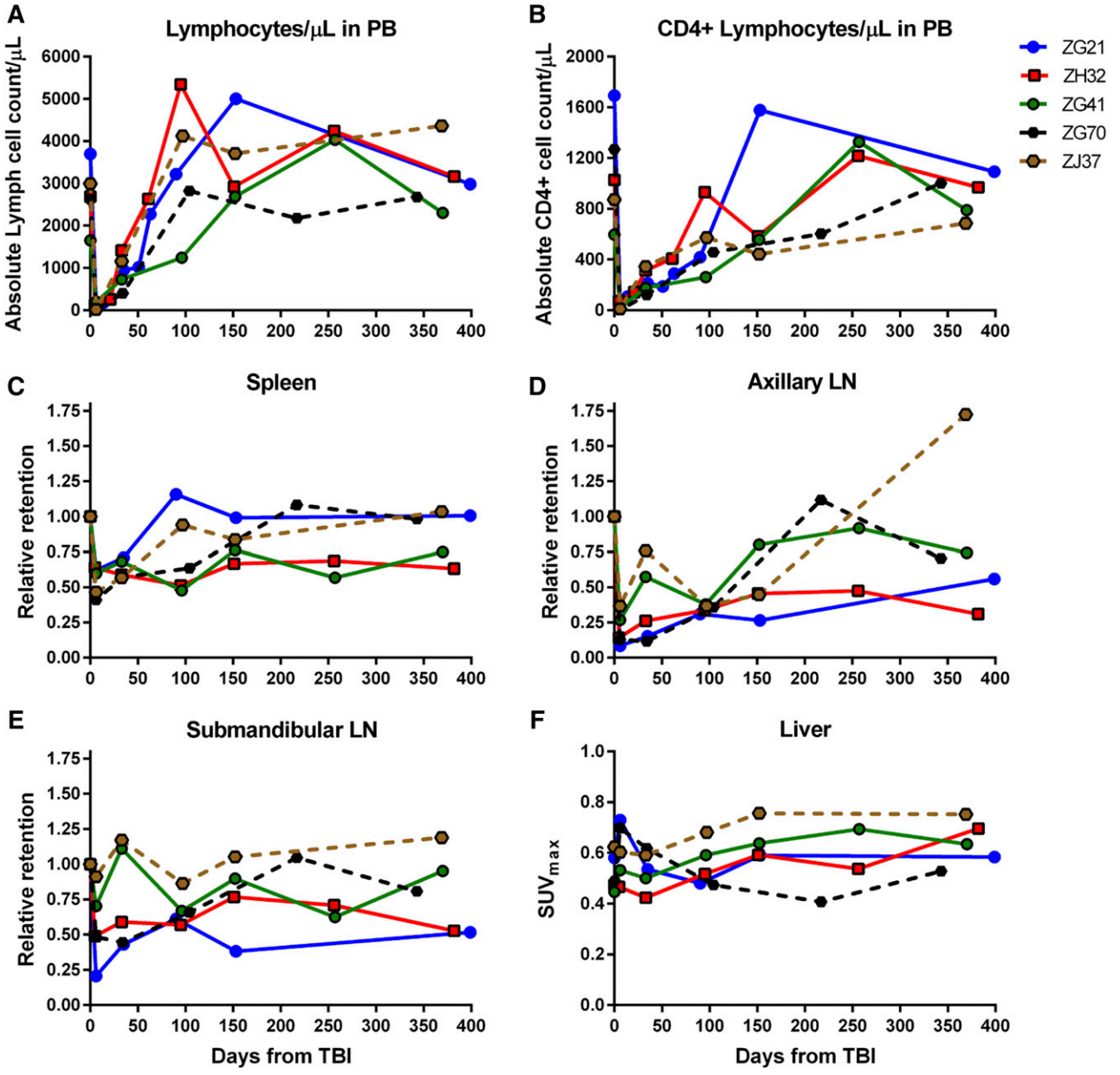

Figure 3. Immune recovery in PB and LTs for 4Gyx2 and 5Gyx2 TBI-transplanted monkeys. The total number of lymphocytes (A) and CD4$^+$ cells (B) in PB, the retention of radiotracer in spleen (C), axillary (D) and submandibular (E) LNs relative to the baseline retention, and the maximum liver (F) SUV for up to 1 year following 4Gyx2 TBI of ZG21 (blue), ZH32 (red), and ZG41 (green) and 5Gyx2 of ZG70 (black dash) and ZJ37 (brown dash) rhesus macaques.

At 4Gyx2 TBI, SPECT imaging was evaluated longitudinally (Figure 1C). At day 6 post-TBI, flow cytometric analysis of the PB showed that all 3 monkeys experienced dramatic depletion of PBLs (88%-95% depletion) and CD4$^+$ lymphocytes (93%-97% depletion) (Figure 3). SPECT imaging, however, revealed variability in LT CD4 depletion between and within hosts (Figure 4), with more dramatic decreases observed in axillary LNs (73%-92%) and milder decreases in the spleen (36%-40%). This could be compared with the more profound LT depletion observed in a chronically coinfected SIV/SHIV rhesus macaque (G43). This difference is seen on the fusion image of SPECT and CT views showing the radiotracer retention in the spleen of ZG21 at baseline and day 6 post-TBI, with nearly complete depletion in chronically SHIV/SIV-infected G43 (supplemental Figure 5).

The recovery of the CD4 pool in tissues appeared overall slower than the recovery of CD4 cells in the PB, suggesting that changes in trafficking rates between LTs and PB play a role in transplant recovery. By month 9 post-TBI, 1 animal (ZG41) had full recovery of the PB CD4$^+$ Lc count and the CD4 pool in axillary LNs quantified by SPECT/CT imaging, but minimal recovery of CD4 pools was observed in the spleen. In another animal (ZG21), full recovery of the PB CD4$^+$ cell count was observed by month 5 concomitant with full recovery of the spleen CD4 pool, despite still >70% depletion of CD4 pool in axillary LNs. In the last animal (ZH32), by month 3, the CD4$^+$ lymphocyte count in PB was fully recovered, however, minimal CD4 pool recoveries were observed in LT through 1 year post-TBI. Overall, in vivo imaging revealed suboptimal reconstitution of the CD4 pool in axillary LNs 1 year from TBI (mean 54% recovery from baseline),

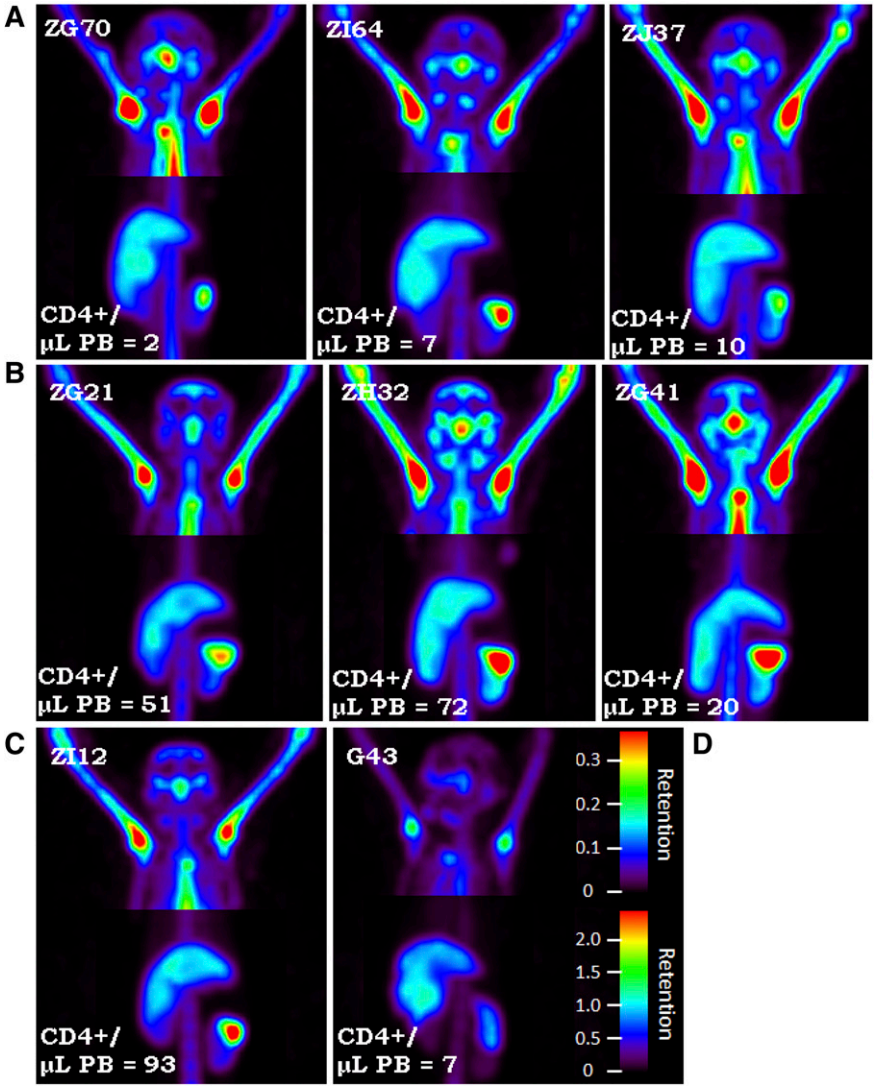

Figure 4. SPECT maximum intensity projection images. SPECT maximum intensity projection images comparing (C) 3Gyx2 (ZI12), (B) 4Gyx2 (ZG21, ZH32, ZG41), and (A) 5Gyx2 (ZG70, ZI64, and ZJ37) at day 6 post-TBI and (D) a chronically infected SHIVDH12R/SIVmac239 rhesus macaque (G43). Despite low circulating levels of $CD4^+$ cells in all animals, residual $CD4^+$ cells remain within LT such as the spleen following TBI, but more profound depletion is associated with chronic SHIV infection. Different image contrasts were applied to head and abdominal field of views to highlight clusters of LNs and spleen. Grayscale images were converted to rainbow colors with appropriate retention scales, where red color indicates high retention.

consistent with LN immunohistochemistry (IHC) data (supplemental Figure 6).

Splenic resistance to irradiation was also observed in the 5Gyx2 animals imaged at day 6 post-TBI, with the maximum depletion (59%) observed in ZG70 (Figure 4), yet not as dramatic as the depletion observed in the cluster of LNs in the TBI animals or as dramatic as the depletion observed in the spleen of a SIV/SHIV chronically coinfected animal (G43) with similar low CD4 counts in the PB. ZI64 was euthanized immediately following imaging at day 6 post-TBI, and IHC for CD3 expression in LTs of ZI64 (Figure 5) correlated with the SPECT imaging in that residual $CD3^+$ lymphocytes were found in the spleen, while there was complete disruption of LN architecture.

By grouping all animals imaged at day 6 post-TBI, a statistically significant decrease in radiotracer retention is observed in the axillary LNs ($P = .003$, n = 7), submandibular LNs ($P = .016$, n = 7), and spleen ($P < .001$, n = 7); by limiting the analysis to the animals imaged up to month 6 post-TBI, we still find a statistically significant lower uptake in the axillary LNs compared with baseline levels ($P = .029$, n = 5).

The 2 long-term transplanted animals (4 and 4.2 years from 5Gyx2 TBI) showed whole-body distribution of the CD4 pool similar to healthy controls, with 1 animal showing radiotracer retention in the cluster of LNs still low compared with healthy controls (supplemental Figure 7). In addition, both of these monkeys developed an antibody response to the radiotracer following a single exposure.

Of particular interest was the discordance between rapid recovery of $CD4^+EGFP^-$ lymphocytes and the delayed appearance of $CD4^+EGFP^+$ lymphocytes (Figure 6). This contrasts with $CD20^+$ lymphocytes whose PB numbers were more effectively depleted with irradiation and $EGFP^+$ and $EGFP^-$ subsets recovered virtually in unison (Figure 6). Based on EGFP expression, it appears to take longer for transplanted $CD34^+$ cells to contribute to some lineages (CD4) than others (CD20). The more rapid reappearance of $CD4^+EGFP^-$ than $CD4^+EGFP^+$ numbers may be a result of endogenous recovery of $CD4^+$ cells from TBI-resistant reservoirs such as the spleen.

Discussion

Little is known about the extent of total body LT damage and recovery following TBI. Most of what is known is based on invasive procedures requiring either biopsy, or necropsy, and/or studies of PB. It has been shown that clonable, alloreactive T cells could be isolated from the spleens of rhesus macaques following hyperfractionated TBI and

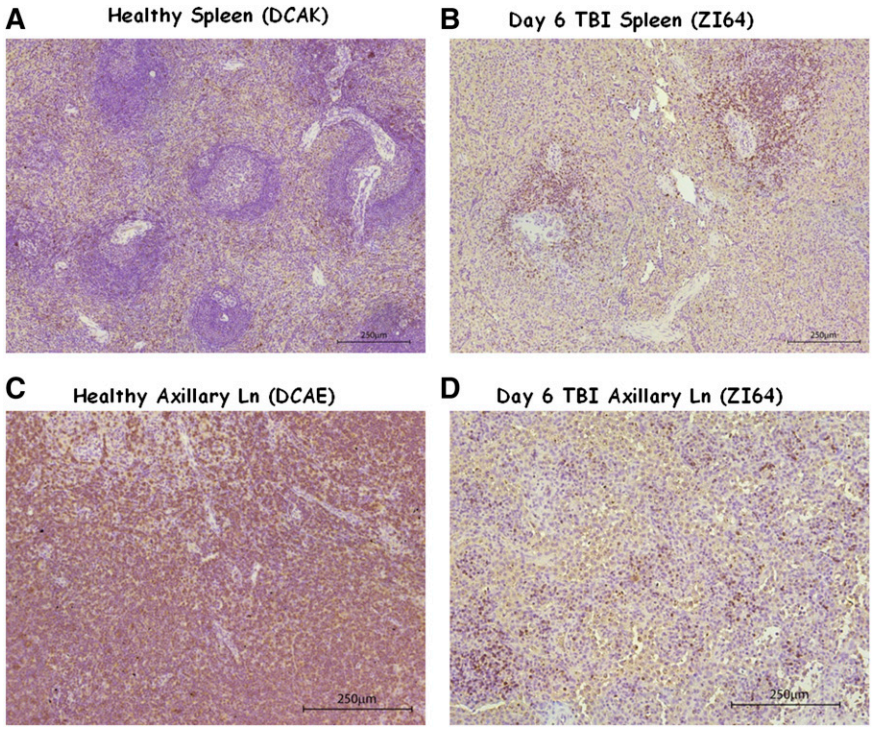

Figure 5. IHC of healthy and day 6 post TBI spleen and axillary LN tissues. (A-B) The comparison of spleen tissue stained for $CD3^+$ cells in (A) a healthy control (DCAK) to (B) a 5Gyx2 monkey euthanized on day 6 post-TBI (ZI64). Residual lymphocytes (stained with a rabbit polyclonal anti-human CD3 antibody) were observed within the spleen but with a complete disruption of LN architecture in ZI64. (C-D) A similar comparison of axillary LN. These ex vivo data correlates with the SPECT imaging.

chemotherapy.[5] This is problematic if one is concerned about residual disease, endogenous contributions to recovery, and/or graft-versus-host disease. Here, we have developed a noninvasive means of evaluating LT recovery following TBI. We tested this approach in a large animal model using SPECT/CT imaging on rhesus macaques receiving various doses of TBI and HSCT using autologous $CD34^+$ cells transduced with a chimeric lentiviral vector expressing the EGFP transgene marker. At a TBI dose of 3Gyx2, both the radiotracer and transgene proved immunogenic. At 4Gyx2, however, longitudinal studies could be performed for at least 1 year using the radiotracer until, in all cases, the animals developed an immune response to the tracer despite a continued tolerance to EGFP expression. Similarly, for 5Gyx2, at 1.5 years an immune response was detected to the radiotracer with continued expression of EGFP. This suggests that tolerance can be successfully achieved to an antigen which is continually expressed,[13] however, intermittent exposure to an antigen, in this case the radiotracer, although delayed, will become immunogenic upon immune recovery of the transplanted animal. Our findings demonstrate a clear difference between continued and intermittent exposure to an antigen and its immunogenicity in the transplant setting. Whereas animals develop tolerance to EGFP, intermittent exposure to the radiotracer remained immunogenic upon immune recovery.

Surprisingly, SPECT/CT imaging revealed significant retention of $CD4^+$ cells within immune tissues at day 6 post-TBI at all doses examined. This was despite a dramatic reduction in $CD4^+$ lymphocytes in the circulation. Flow cytometric analysis of PB revealed a residual population of $CD4^+$ cells following TBI, but a >99% depletion of $CD20^+$ cells. More dramatic decreases of $CD4^+$ cells for the 4Gyx2 TBI group were observed in axillary LNs (73%-92%) than in the spleen (36%-40%). Thus, it appears the spleen remains a significant reservoir of $CD4^+$ lymphocytes following TBI. The novel anti-CD4 radiotracer used in this study cannot discriminate between $CD4^+$ T cells and other $CD4^+$ cells such as macrophages. The latter cells, however, express CD4 at relatively low levels per cell compared with lymphocytes.[14,15] Moreover, the percentage of mononuclear cells that are macrophages is much lower than lymphocytes in spleen and LNs.[16] Hence, the contribution to the total binding sites for the radiotracer, that is, CD4 receptors per unit mass/volume of tissue, brought by the macrophages/monocytes compartment is expected to be much lower than the contribution brought by the $CD4^+$ T cells. This is corroborated by the IHC conducted on $CD3^+$ cells which shows evidence of a substantial pool of T cells that survive the TBI in the spleen but not in the LNs, consistent with the imaging data presented in this study.

A clear discordance was noted between PB and LTs in $CD4^+$ cell recovery. The PB $CD4^+$ lymphocyte count returned to baseline within 4 to 9 months for the 4Gyx2 TBI group, however, in vivo imaging revealed suboptimal reconstitution of the $CD4^+$ cell pool in axillary LNs even at 1 year from TBI (mean 54% recovery from baseline). This was consistent with IHC evaluated at 1 year post-TBI in the 3 4Gyx2 monkeys (supplemental Figure 5). Peripheral LNs appear to be particularly damaged following TBI and may never fully recover despite a normalized circulating $CD4^+$ lymphocyte cell count. Although at 5Gyx2 SPECT/CT imaging revealed a more severe depletion of $CD4^+$ cells in LTs, $CD4^+$ lymphocyte cells could still be observed in the spleen. Of particular interest was the discordance between rapid recovery of $CD4^+EGFP^-$ lymphocytes and the delayed appearance of $CD4^+EGFP^+$ lymphocytes. This contrasts with $CD20^+$ lymphocytes in which $CD20^+EGFP^+$ and $CD20^+EGFP^-$ subsets that were more effectively depleted by irradiation recovered simultaneously. Thus, lymphocyte subset and LT sensitivity to irradiation appear to differ in recovery kinetics.

Our results present for the first time a noninvasive method in real time to evaluate $CD4^+$ cell immune recovery in LTs following HSCT using SPECT/CT imaging. Despite close to complete ablation of circulating leukocytes following TBI, we did not observe total depletion of $CD4^+$ cells in LTs such as the spleen. This study advances the field of molecular imaging in being able to longitudinally follow lymphoid recovery following TBI and will permit investigators to evaluate in real time the extent of CD4 immunosuppression following a variety of therapeutic regimens and disease states, such as those associated with viral infections. As imaging technology advances, so

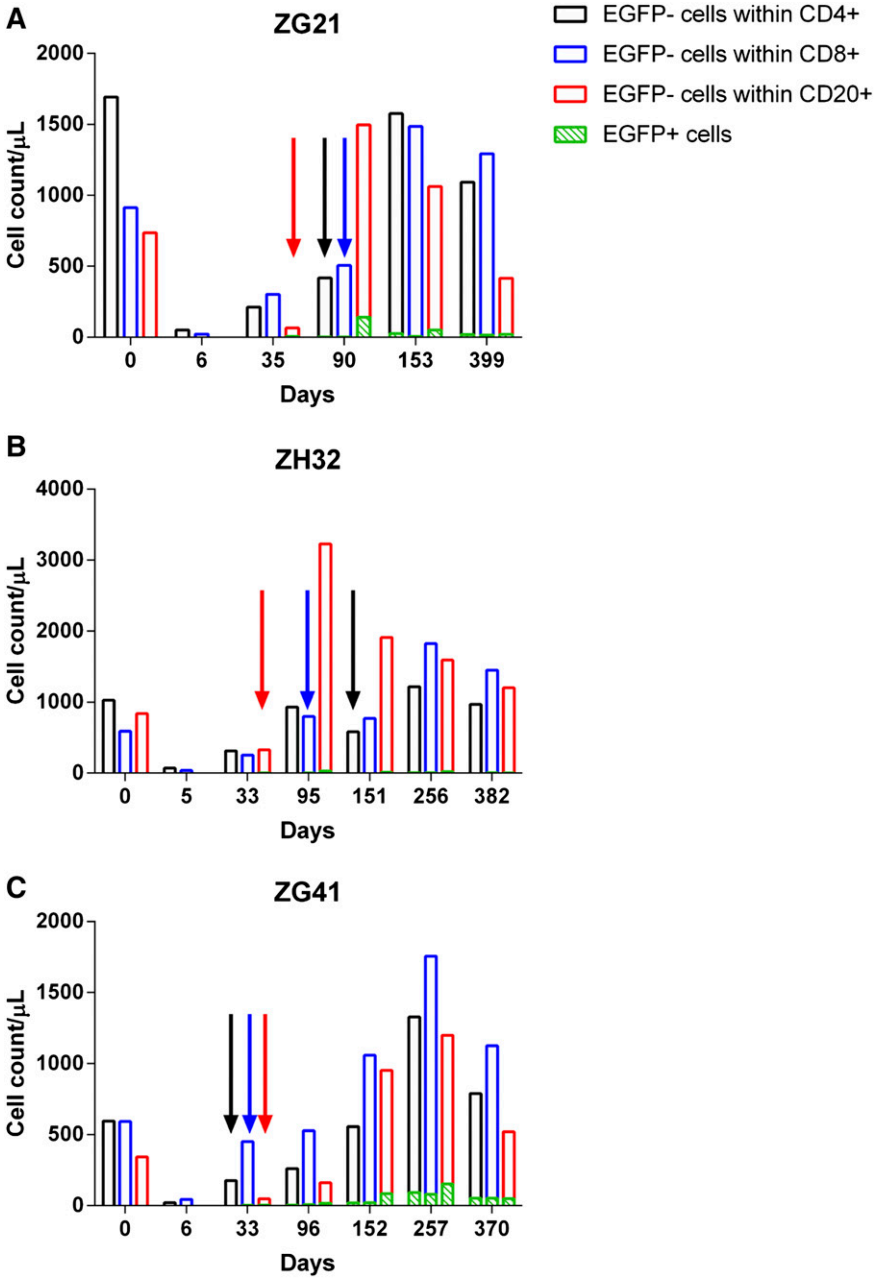

Figure 6. Lymphocyte recovery posttransplant. (A-C) CD4 (black), CD8 (blue), and CD20 (red) lymphocyte recovery and EGFP expression (green) for the 4Gyx2 TBI transplanted monkeys over time. The colored arrows represent the first detectable appearance of their respective $EGFP^{+}$ subset.

does its potential. The recovery of other hematopoietic subsets besides CD4 can be monitored following transplant. The location and therapeutic role of specific cell types in cellular or immunotherapies can be evaluated. Reservoirs of cells in LT of patients undergoing allogeneic transplantation can be followed in real time for either graft rejection or graft-versus-host disease and treated early. In addition, an investigator can therapeutically either accelerate or deter the expansion of a particular cellular subset and monitor the treatment's success. Still, work needs to be done. Clearly, avenues need to be explored and developed to avoid immune responses to the radiotracer so that sequential imaging can be performed safely without the need of TBI. Along with pioneering attempts to provide noninvasive imaging to determine antiretroviral drug penetration[17] or SIV viral replication,[18] the methodology behind whole-body pharmacodynamics has advanced significantly in the past decade, appearing less futuristic.

Acknowledgments

The authors thank the animal care staff and technicians at 5 Research Court, and the Division of Veterinary Resources, National Institutes of Health (NIH) for their excellent care and handling of the animals. The authors also thank Drs Marlene Orandle and Michael Eckhaus and his staff for assisting in the pathologic interpretation of the LT IHC; William DeGraff and Dr Jim Mitchell of the Radiation Biology Branch, National Cancer Institute (NCI) for the use of the Eldorado Cobalt-60 irradiator; Dr Kenneth Cheng of the Clinical Center for radiopharmacy support; and the staff at the Armed Forces Radiation Research Institute (AFRRI), Bethesda for the use of their Cobalt-60 irradiator.

This work was supported by the intramural research program of the National Heart, Lung, and Blood Institute (NHLBI), the National Institutes of Allergy and Infectious Diseases (NIAID), and the

National Institute of Diabetes, Digestive, and Kidney Diseases (NIDDK) at the National Institutes of Health (NIH). This project has been funded in part with federal funds from the National Cancer Institute (NCI), NIH, under contract no. HHSN261200800001E.

Authorship

Contribution: R.E.D., S.S., and M.D.M. designed and performed the research, analyzed/interpreted the data, made the figures, and co-wrote the paper; M.E.M. and A.E.K. performed transplants and provided animal support; A.C.B., C.H.P., I.K., A.S.C., G.D., P.D., and M.S.C. performed research and analyzed/interpreted data; R.C.R. analyzed/interpreted data; N.U. supplied chimeric lentiviral vector and performed transductions; H.C.L. and J.F.T. designed research and analyzed/interpreted data; and all co-authors critically reviewed the paper.

Conflict-of-interest disclosure: The authors declare no competing financial interests.

Correspondence: Robert E. Donahue, Hematology Branch, National Heart, Lung, and Blood Institute, MSC 4450, 49 Convent Dr, Bethesda, MD 20892-4450; e-mail: donahuer@nhlbi.nih.gov.

References

1. Westermann J, Pabst R. Distribution of lymphocyte subsets and natural killer cells in the human body. *Clin Investig.* 1992;70(7):539-544.
2. Donahue RE, Kuramoto K, Dunbar CE. Large animal models for stem and progenitor cell analysis. *Curr Protoc Immunol.* 2005;Chapter 22: Unit 22A.
3. Uchida N, Washington KN, Hayakawa J, et al. Development of a human immunodeficiency virus type 1-based lentiviral vector that allows efficient transduction of both human and rhesus blood cells. *J Virol.* 2009;83(19):9854-9862.
4. Di Mascio M, Paik CH, Carrasquillo JA, et al. Noninvasive in vivo imaging of CD4 cells in simian-human immunodeficiency virus (SHIV)-infected nonhuman primates. *Blood.* 2009;114(2):328-337.
5. Reisner Y, Ben-Bassat I, Douer D, Kaploon A, Schwartz E, Ramot B. Demonstration of clonable alloreactive host T cells in a primate model for bone marrow transplantation. *Proc Natl Acad Sci USA.* 1986;83(11):4012-4015.
6. Pulito VL, Roberts VA, Adair JR, et al. Humanization and molecular modeling of the anti-CD4 monoclonal antibody, OKT4A. *J Immunol.* 1996;156(8):2840-2850.
7. Padlan EA. Anatomy of the antibody molecule. *Mol Immunol.* 1994;31(3):169-217.
8. Lindmo T, Bunn PA Jr. Determination of the true immunoreactive fraction of monoclonal antibodies after radiolabeling. *Methods Enzymol.* 1986;121:678-691.
9. Di Mascio M, Srinivasula S, Kim I, et al. CD4 T cell reconstitution following cART is immediate as is CD4+ T cell depletion following treatment interruption: coupling the whole-body imaging of the CD4 pool and of the immune system activation [abstract]. Vancouver, BC, Canada: . International AIDS Society. Abstract WelbPe06; 2015.
10. Kean LS, Sen S, Onabajo O, et al. Significant mobilization of both conventional and regulatory T cells with AMD3100. *Blood.* 2011;118(25):6580-6590.
11. Uchida N, Weitzel RP, Platner C, et al. Myeloablative conditioning is required for efficient engraftment of gene-modified cells and prevention of antibody production against transgene products in a rhesus stem cell gene therapy model [abstract]. New Orleans, LA: American Society of Gene & Cell Therapy; 2015. Abstract 294.
12. Uchida N, Weitzel RP, Evans ME, et al. Evaluation of engraftment and immunological tolerance after reduced intensity conditioning in a rhesus hematopoietic stem cell gene therapy model. *Gene Ther.* 2014;21(2):148-157.
13. Kung SK, An DS, Bonifacino A, et al. Induction of transgene-specific immunological tolerance in myeloablated nonhuman primates using lentivirally transduced CD34+ progenitor cells. *Mol Ther.* 2003;8(6):981-991.
14. Lewin SR, Sonza S, Irving LB, McDonald CF, Mills J, Crowe SM. Surface CD4 is critical to in vitro HIV infection of human alveolar macrophages. *AIDS Res Hum Retroviruses.* 1996;12(10):877-883.
15. Thomas ER, Dunfee RL, Stanton J, et al. Macrophage entry mediated by HIV Envs from brain and lymphoid tissues is determined by the capacity to use low CD4 levels and overall efficiency of fusion. *Virology.* 2007;360(1):105-119.
16. Blackley S, Kou Z, Chen H, et al. Primary human splenic macrophages, but not T or B cells, are the principal target cells for dengue virus infection in vitro. *J Virol.* 2007;81(24):13325-13334.
17. Di Mascio M, Srinivasula S, Bhattacharjee A, et al. Antiretroviral tissue kinetics: in vivo imaging using positron emission tomography. *Antimicrob Agents Chemother.* 2009;53(10):4086-4095.
18. Santangelo PJ, Rogers KA, Zurla C, et al. Whole-body immunoPET reveals active SIV dynamics in viremic and antiretroviral therapy-treated macaques. *Nat Methods.* 2015;12(5):427-432.